Vertically stacked short channel $PtSe_2$/ultrathin-Silicon heterojunction for fast-speed UV photodetection application

Jiang Wang[1], Jiangxu Yang[1], Bo Yu[1], Zhicheng Wu[1], Mengting Jiang[2], Chun-Yan Wu[1], Yang Wang[1], Feng-Xia Liang[1], Xuezhi Ma[2, 3], Li Li[4], Lin-Bao Luo[1, *]*

[1] School of Microelectronics, Hefei University of Technology, Hefei, Anhui 230009, China.

*[2] Institute of Materials Research and Engineering (IMRE), Agency for Science, Technology and Research (A*STAR), 2 Fusionopolis Way, Innovis, #08-03, Singapore 138634, Republic of Singapore.*

*[3]Quantum Innovation Centre (Q. InC), Agency for Science, Technology and Research (A*STAR), 2 Fusionopolis Way, Innovis, #08-03, Singapore 138634, Republic of Singapore.*

[4] China Resources Microelectronics (Chongqing) Limited, Chongqing 401332, China.

Corresponding authors. E-mail: maxuezhi@imre.a-star.edu.sg (Xuezhi Ma), luolb@hfut.edu.cn (Lin-Bao Luo)

Abstract

Superior ultraviolet photodetectors (UVPDs) with fast response speed and high responsivity are essential for UV communication, intelligent sensing, advanced manufacturing, and more. Various studies have demonstrated the excellent performance of traditional UVPDs based on wide bandgap semiconductors (WBSs). However, these devices often suffer from a relatively slow response speed due to the defect states within WBSs. In this work, we developed a new short channel non-WBS UVPD using the vertically stacked short channel $PtSe_2$/ultrathin-Si UVPD. The heterojunction is stacked by the 200nm thick Si flake that exfoliated from a Silicon-on-Insulator (SOI) wafer by wet etching and the wafer-scale CVD -grown $PtSe_2$ via the mature PDMS stamp transfer protocols. The absorption in the Si layer, which depends on the incident wavelength, shows a strong correlation with the device photocurrent response. Under 365 nm illumination, the vertical device exhibits a fast UV response speed up to 51.8/73.6 μs, respectively. This performance outperforms that of conventional lateral structures and many WBS-based UVPDs, largely attributed to the extremely short transport distances of photogenerated carriers and the superior physical characteristics of Si. This study shows that ultrathin-Si is a promising building block for fast speed UVPDs, which are vital for UV optoelectronic applications.

Introduction

Ultraviolet (UV) radiation constitutes approximately 10% of the total solar spectrum, has been researched since the 19th century, initially focusing specifically on the invisible radiation beyond blue light.[1] Over the past few decades, the rapid development of the electronics industry has greatly advanced UV radiation application and detection technologies, particularly in sterilization, spectral analysis, UV curing, and other areas.[2-5] Ultraviolet photodetectors (UVPDs) are used to convert UV light signals into electrical signals enabling the analysis of UV radiation levels. Compared to infrared PDs, UVPDs are unaffected by long-wavelength electromagnetic waves, providing superior concealment, thermal stability, and reliability, which secures their crucial role in both civil and military fields.[6, 7]

Conventionally, the majority of commercial UVPDs are fabricated by using wide bandgap semiconductor (WBS) materials as photoactive materials ($E_g > 2$ eV),[1, 8] including ZnO (3.37 eV),[9] ZnS (3.7 eV),[10] ZnSe (2.7 eV),[11] GaN (3.4 eV),[12] diamond (5.5 eV),[13] Ga_2O_3 (4.8 eV),[14] and their ternary alloys such as $Al_xGa_{1-x}N$,[15] $Mg_xZn_{1-x}O$,[16] ZnS_xSe_{1-x},[17] etc. These WBS materials exhibit excellent chemical stability, high electron drift velocity, and appropriate cut-off wavelength in the UV spectrum. Although it is possible to grow wafer-scale binary WBSs using metal organic chemical vapor deposition (MOCVD) and molecular beam epitaxy (MBE), there are still substantial bottlenecks in the flexibility of large-area integrated device fabrication due to the lattice mismatch, complementary metal oxide semiconductor (CMOS) incompatibility and other problems.[18, 19] In addition, the epitaxial growth of ternary alloy semiconductors requires stringent conditions and is susceptible to phase segregation at high compositional ratios, which hinders the fabrication of high-performance UVPDs.[20, 21] While bulk WBSs-based UVPDs based on show excellent performance, including high responsivity Ga_2O_3 single crystal field-effect phototransistors,[22] $Al_{0.3}Ga_{0.7}N$/GaN phototransistor,[12] and Ga_2O_3 vertical Schottky phototransistor,[23] the photoresponse performance of these devices generally decreases as the material thickness is reduced, primarily due to the low optical absorption rate and defect trapping states of the ultra-thin WBSs.[19, 24] Nevertheless, the development of the devices with fast response speed remained an important challenge in many types of UVPDs. The above issues of WBS lead to a slow response speed of the device.

Besides the WBSs, some narrow bandgap semiconductors are also used in UVPDs. However, their

larger channels caused by the fabrication process, along with prevalent defect states and recombination centers in these semiconductors lead to slower response speed of the device.[25, 26] Some scale-dependent semiconductor materials (thickness or diameter) not only have high crystalline quality but also offer effective UV detection.[25, 27] These small-scale semiconductor materials interact with light in ways that differ significantly from their bulk counterparts.[26] Recently, thickness-dependent non-WBSs have also recently achieved high-performance UV detection. For example, the layer-dependent β-Te has shown a decent DUV response at a relatively small thickness of ~ 18.9 nm.[28] Additionally, in a Si-nanowires (Si NWs) PD, when the diameter of metal-assisted etched Si NWs decreased to 36 nm, the responsivity under 300 nm illumination reached up to 10.2 A/W.[29] The channel length in vertically structured devices is determined by the thickness of the semiconductor, is typically short. This reduction in channel lengths can significantly suppress the additional resistance and shorten the carriers transit time, thereby improving the photocurrent and response speed of the device (Figure 1a).[30]

Among most of the semiconductors, Si is one of the most ideal materials and plays the pivotal position in the fields of electronics and optoelectronics due to its excellent optical and electrical properties, mature preparation processes, and abundant natural resources.[31, 32] In recent years, Si provides an effective platform for the realization of readout circuits for PDs, Si-based optoelectronics have successfully achieved high-performance, highly stable and low-cost photonic integrated circuits because of its CMOS compatibility.[33, 34] Moreover, empirical evidence demonstrates that the penetration depth of light in Si decreases sharply with decreasing wavelength. Notably, the penetration depth of UV light with a wavelength of less than 360 nm is only 20 nm. The region beyond the penetration depth acts like a series resistor, significantly effecting carriers transport and photocurrent. Importantly, the commercially mature SOI provides the opportunity for the readily available thin wafer-scale Si single crystal film for a vertical device.

In this study, we demonstrate a vertically stacked $PtSe_2$/ultrathin-Si heterostructure based UVPD using the narrow bandgap semiconductor and achieved high responsivity and fast response speed. The ultrathin-Si flacks were exfoliated from SOI wafers by the standard wet etching,[35] and the $PtSe_2$ nanofilms were directly selenized from the electron beam evaporated Pt film. The stacking of ultrathin-Si and $PtSe_2$ were accomplished through a mature dry transfer method, ensuring high reproducibility and consistent performance. Under UV to NIR illumination, the peak photocurrent of the device occurs

in the UV band. Theoretical simulations showed that ultrathin-Si has strong absorption of UV light due to the high absorption coefficient of Si in the UV region. Device analysis revealed that the device exhibits a high peak responsivity of 1.11 A/W under 365 nm illumination. Compared with many WBSs based UVPDs, the vertically stacked $PtSe_2$/ultrathin-Si heterojunction exhibits a fast response speed of 51.8/73.6 μs owing to the shorter channel of photogenerated carriers transport. We believe that this fast Si-based UVPD holds promising application prospects in future UV optoelectronics.

Results and Discussion

Figure 1b shows the fabrication process of the $PtSe_2$/ultrathin-Si UVPD. Here, the ultrathin-Si was obtained by wet etching an SOI substrate. The SOI substrate was first cleaned and then etched in a 5% HF solution for 1h. The etched top-Si was subsequently dispersed onto a clean SiO_2 substrate. The $PtSe_2$/ultrathin-Si UVPD was then assembled using PDMS dry transfer, followed by electron beam evaporation to deposit the electrodes (see the Experimental Section for more details). Figure 1d presents (i) the AFM image of $PtSe_2$ with a surface roughness of ~0.6 nm, (ii) the exfoliated top-Si from the SOI with a thickness of ~200 nm, and (iii) is the optical images of patterned Pt and $PtSe_2$ before and after selenization, which show obvious differences. Figure S2 displays the Raman spectrum of $PtSe_2$ nanofilm, with two typical scattering peaks at 177.6 cm^{-1} (E_g) and 206.7 cm^{-1} (A_{1g}) corresponding to the in-plane and out-of-plane vibration modes of $PtSe_2$, respectively.[36, 37] EDS analysis was conducted to determine the elemental composition of $PtSe_2$ nanofilm, revealing an atomic ratio Pt/Se of approximately 2 (Figure S3). These characterizations confirm that high-quality of patterned $PtSe_2$ nanofilms were successfully produced through the post-selenization method.

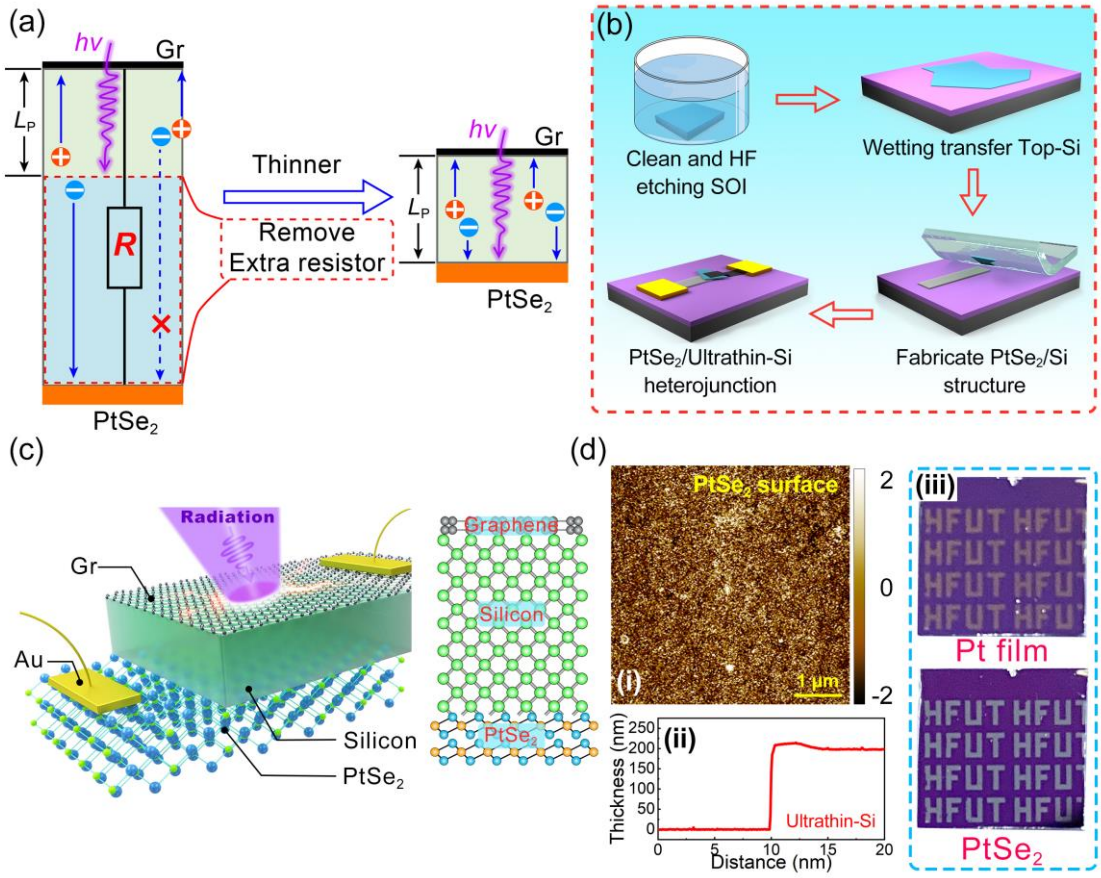

Figure 1. (a) The concept of enhancing UVPD performance through the thinning process. (b) Fabrication process schematic diagram of $PtSe_2$/ultrathin-Si UVPD. (c) Device structure of vertical $PtSe_2$/ultrathin-Si UVPD. (d) AFM image shows surface roughness of $PtSe_2$ nanofilm (i), the thickness of the exfoliated ultrathin-Si (ii), and the optical image of patterned $PtSe_2$ before and after selenization (iii).

To evaluate the optoelectronic characteristics of the $PtSe_2$/ultrathin-Si UVPD, the photoresponse of the device in dark conditions and illumination at various wavelengths was analyzed. Figure 1c shows a schematic of the device, which consists of patterned $PtSe_2$, ultrathin-Si, and few layer graphene (Gr, serves as the top electrode), with 50 nm Au film used as the contact electrodes, and this application of graphene was also reported in other studies on photodetectors[38]. Figure 2a displays the optical image of the device, where a top layer of h-BN isolates it from air. In dark conditions, the device exhibits significant rectification characteristics, which is mainly resulting from the Schottky junction formed between $PtSe_2$ and Si. (Figure 2b) Moreover, under illumination at different wavelengths (1.5 mW/cm^2), the reverse photocurrents of the device initially increase and then decrease, as depicted in

Figure 2c. Then, the absolute values of the photocurrents at a -0.5 V bias were extracted. Figure 2d shows that the increase in photocurrent is predominantly concentrated in the UV region. The peak photocurrent occurs at a wavelength of 365 nm, with the photocurrent of the device gradually decreasing as the wavelength extends from the visible (Vis) to NIR region. This trend is attributed to the varying penetration depths and absorption at different incident wavelengths in Si.[39] Owing to the reduced thickness of the top-Si exfoliated from the SOI, the complete absorption of incident light is predominantly located in the UV band, which promotes a notable UV photocurrent in the device.

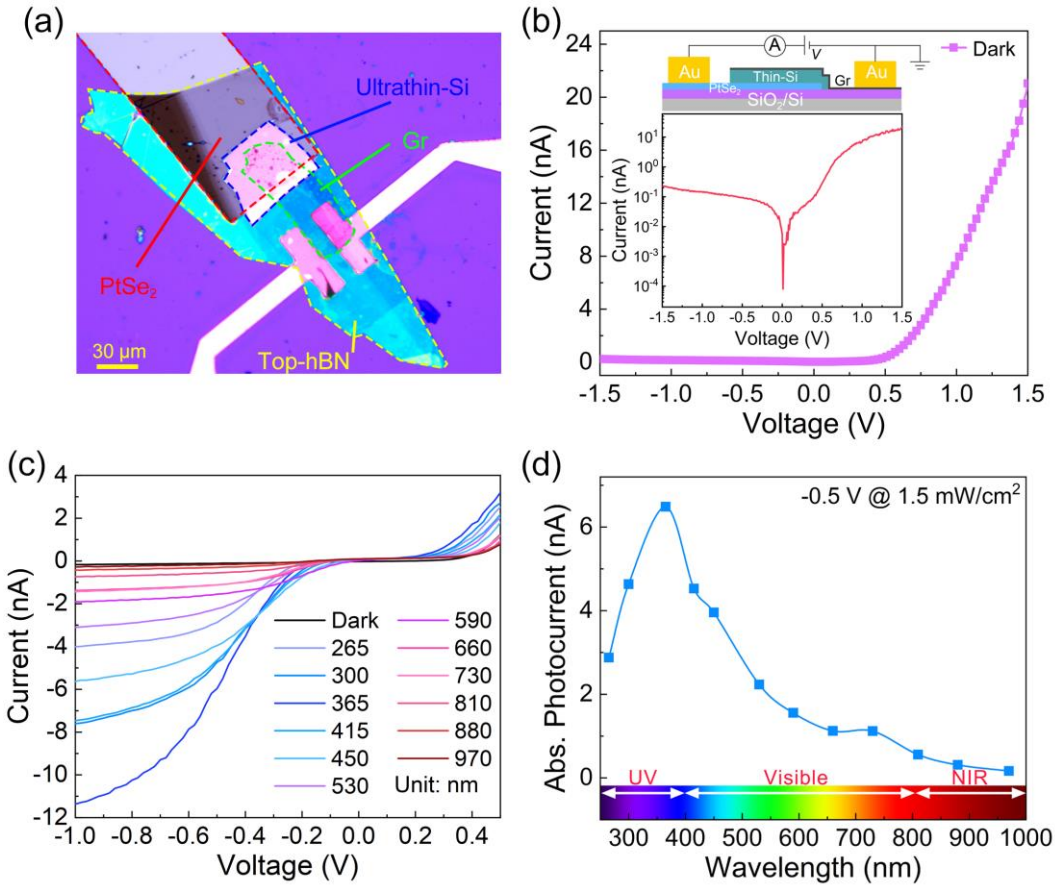

Figure 2. (a) Optical microscope image of a $PtSe_2$/ultrathin-Si UVPD. (b) Current-voltage characteristics of $PtSe_2$/ultrathin-Si UVPD under dark conditions. The inset shows the corresponding log I-V curves and the measurement schematic structure of the device. (c) I-V characteristics of the device measured in the light irradiation (1.5 mW/cm^2) with various wavelengths. (d) The absolute values of the $PtSe_2$/ultrathin-Si UVPD photocurrents extracted at -0.5 V under light illumination at different wavelengths from UV to NIR (1.5 mW/cm^2).

The thickness dependent absorption of the Si that implied the selected thickness is crucial for

determining the peak photoresponse of the device.[39] Consequently, we analyzed the optical and electrical properties of Si at different thicknesses and the $PtSe_2$/ultrathin-Si photodetector through simulations. The results indicate that thinner Si layers predominantly absorb light in the UV band, whereas thicker layers exhibit a broader spectral absorption range, particularly with increased absorption at wavelengths longer than 400 nm (Figure S4a). Additionally, the multiple sharp peaks observed in the absorption arise due to the interference effects of thin Si layer.[40-42] In addition, as shown in Figure 3a, when the Si substrate is irradiated with different wavelengths, the near-surface region of the Si mainly absorbs UV light, which has the shallowest penetration depth among the incident wavelengths. As the incident wavelength increases beyond 400 nm, the absorption rate gradually decreases, while the penetration depth increases. The contour maps in Figure 3b illustrate the changes in photogeneration rate for 200 nm Si under incident light of different wavelengths. It is evident that within this thickness, ultrathin-Si fully absorbs light with wavelengths below 400 nm and exhibits a maximum photogeneration rate. Moreover, as the incident wavelength increases, the ultrathin-Si becomes less effective at absorbing the incident light, leading to a decreased photogeneration rate. Besides, we extracted the photogeneration rate near the surface of the ultrathin-Si (dashed line in Figure 3b), and analysis shows that this rate gradually decreases as the incident wavelength increases from 250 nm to 1.0 μm, with the maximum appearing in the UV band. (Figure S4b) These simulation results align with the trend observed in the peak photocurrent measured in the $PtSe_2$/ultrathin-Si PD. The ultrathin-Si and $PtSe_2$ layers in the $PtSe_2$/ultrathin-Si device exhibit different recombination rates for incident light (Figure 3c). Taking UV incident light (350 nm) as examples, the recombination rate for UV light predominantly occurs in the ultrathin-Si layer because this layer completely absorbs the UV light. However, the recombination rate in the $PtSe_2$ layer becomes significantly lower than in the ultrathin-Si layer under light illumination, due to the diminishing optical absorption in the ultrathin-Si. Notably, simulation revealed that the peak current of the device under different wavelengths irradiation is also centered in the UV region (Figure 3d), which closely corresponds to the experimental results.

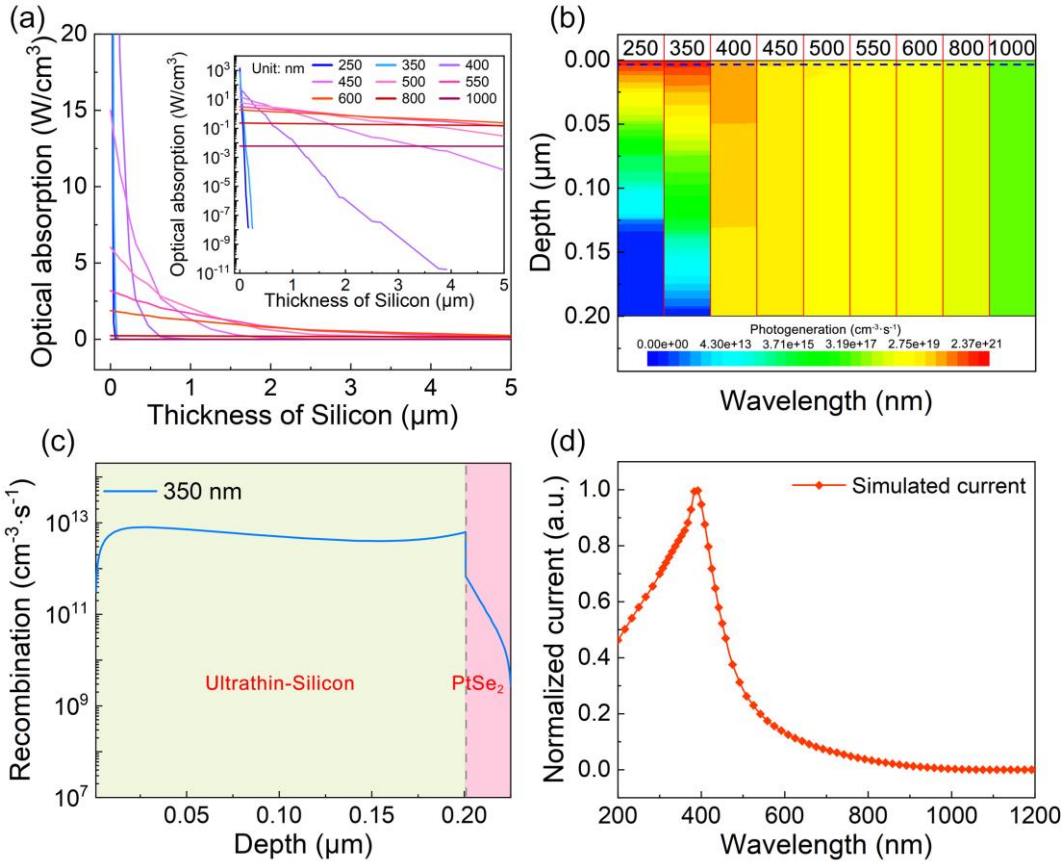

Figure 3. (a) Optical absorption of different incident wavelengths on silicon substrate. (b) Contour maps of photogeneration rate as a function of incident light wavelength and depth in Si. (c) Carrier recombination of $PtSe_2$/ultrathin-Si photodetector. (d) Simulated the near surface current of the device under different wavelength illumination.

In order to benchmark the UV photodetection performance of the vertically stacked $PtSe_2$/ultrathin-Si UVPD, we evaluated the photoresponse of the device under 365 nm light illumination at varying light intensity. Figure 4a displays the I-V characteristics of the device in the dark condition and under 365 nm incident light at different intensities, where the photocurrents under negative bias increase with the incident light intensity rises. Meanwhile, at -0.5 V bias, the photocurrent of the device increases from 0.204 nA to 11.801 nA as the light intensity increases from 0.01 mW/cm^2 to 6 mW/cm^2, and the I_{light}/I_{dark} increases from 2.04 to 118.01, attributing to the increased number of the photo-absorption generated electron-hole pairs within the semiconductor channels. These carriers are effectively separated and collected by the electrodes due to the combined effects of the external voltage and the built-in-electric field, thereby generating the photocurrent.[43, 44] In addition, the photoresponse of the device can be rapidly switched between on and off states under 365 nm on/off light illumination at a -

0.5 V bias (Figure 3b). The relationship between photocurrent and incident light intensity can be fitted with the following formula:[43]

$$I_{ph} = AP^{\theta} \quad (1)$$

Here, A is a wavelength-dependent constant, I_{ph} represents the photocurrent, P is the incident light intensity, and θ is the index that describes the photogenerated carrier generation-recombination processes.[45] The fitting results are shown in Figure 4d, and we determined that the θ exponent for $PtSe_2$/ultrathin-Si UVPD is 0.65. This sublinear relationship stems from the complex process of generation, transport, and recombination of photogenerated carriers in the device, which are fundamentally influenced by the capture centers and interface defect states.[46] As a key parameter for quantitative evaluation of photodetector performance, the photo-responsivity (R) can be expressed as:[47]

$$R = \frac{I_{ph}}{P_{\lambda} \times S} \quad (2)$$

Where P_{λ} is the incident light intensity and S is the effective photosensitive area of the device. Furthermore, external quantum efficiency (EQE) is defined as the ratio of the number of photogenerated carriers (such as recombination processes of photogenerated electron-hole pairs, etc.) collected by the photodetector to the number of incident photons when the incident light irradiates the device, which can be calculated as follows:[48]

$$EQE = R\frac{hc}{e\lambda} \quad (3)$$

Where h, c, e, and λ are the Planck's constant, the speed of light, the electron charge, and the wavelength of the incident light, respectively. As shown in Figure 4c, at -0.5 V, the R of the device is up to 1.11 A/W at a light intensity of 0.01 mW/cm^2. This key value R significantly exceeds that of some UVPDs, such as doped MoS_2/$SnSe_2$ heterojunction,[49] MSM structured GaN,[50] and β-Ga_2O_3/GaN nanowire heterojunction.[51] Nevertheless, the absorption of the channel material to the incident light gradually saturated as the incident light intensity increases, and the recombination of photogenerated electron-hole pairs becomes more evident at higher intensity. These factors cause a steady decline in R with increasing light intensity.[52] Moreover, the obtained EQE values for the $PtSe_2$/ultrathin-Si UVPD at various light intensities are also plotted in Figure 4c, with a maximum value of 377.69% at -0.5 V bias. The high EQE exceeding 100% indicates the existence of internal

gain in the device, which in turn results in carrier multiplication. Compared to lateral devices, the vertical $PtSe_2$/ultrathin-Si structure reduces the transit time (τ_t) of photogenerated carriers. The gain determined by both the photogenerated carrier lifetime (τ_l) and transit time, is described as follows: $G = \tau_l/\tau_t$.[45, 53] Also, the external bias enhances the electric field, which facilitates the impact ionization of carriers, thus also contributing to the gain.[54, 55]

We calculated the photo-responsivity for different incident wavelengths based on the preceding photoresponse analysis results of the device in the UV-NIR range (Figure 4e), and it can be seen that the variation trend matched the photocurrents. We measured the noise power density of the device under dark conditions, as shown in Figure 4f, where the primary noise source at low frequency waves is 1/f noise, originating from contact interfaces and defect states.[56, 57] Moreover, it also can be seen from Figure 4f, the noise power density of the device is 2.5×10^{-14} A/Hz$^{1/2}$ under 1Hz. Furthermore, the noise equivalent power (NEP) can be calculated by: $NEP = I_{noise}/R$, and the specific detectivity can be obtained by[58]:

$$D^* = \frac{\sqrt{S\Delta f}}{NEP} \quad (4)$$

Under -0.5 V and 365 nm light illumination with the light intensity increases from 0.01 mW/cm^2 to 6 mW/cm^2, the NEP and D^* changes from 2.25×10^{-14} W/Hz$^{1/2}$ to 1.3×10^{-13} W/Hz$^{1/2}$, and 1.36×10^{11} Jones to 2.35×10^{10} Jones, respectively. Figure 4g presents the approximate resistance distribution in vertically stacked $PtSe_2$/ultrathin-Si UVPD, while Figure S5a shows the resistance distribution of traditional lateral heterojunctions. These components mainly include the $PtSe_2$/ultrathin-Si interface resistance (R_j), the series resistance of Si and $PtSe_2$ outside the junction (R_s and R_m), the contact resistance of Au/ $PtSe_2$ and Si/Gr (R_{cm} and R_{cs}). In the vertical $PtSe_2$/ultrathin-Si UVPD, carriers only traverse the thin ultrathin-Si channels, with Gr exhibiting extremely low resistance. However, the series resistance (R_s) outside the junction region substantially influences carriers transport in the lateral structure. This significantly reduces the photoresponse performance of the device under UV illumination. (Figure S5c-d). In contrast, the long distance in lateral device prolongs the transition time for photogenerated carriers, which hinders fast photoresponse. Figure 4h displays the simulated electric field distribution of $PtSe_2$/ultrathin-Si, the large electric field intensity is principally concentrated near the junction interface on the Si side. The arrows in the figure indicate the direction of the total current flow. To explain the carrier transport mechanism in the device, Figure 4i presents

the energy band alignment diagram of $PtSe_2$/ultrathin-Si. After $PtSe_2$ and Si come into contact and reach equilibrium, a space charge region forms at the interface, and the resulting built-in electric field facilitates the drift and diffusion of carriers. Under UV illumination, the photogenerated electron-hole pairs are effectively separated by the built-in electric field and external bias and are eventually collected by the electrodes.[21, 52]

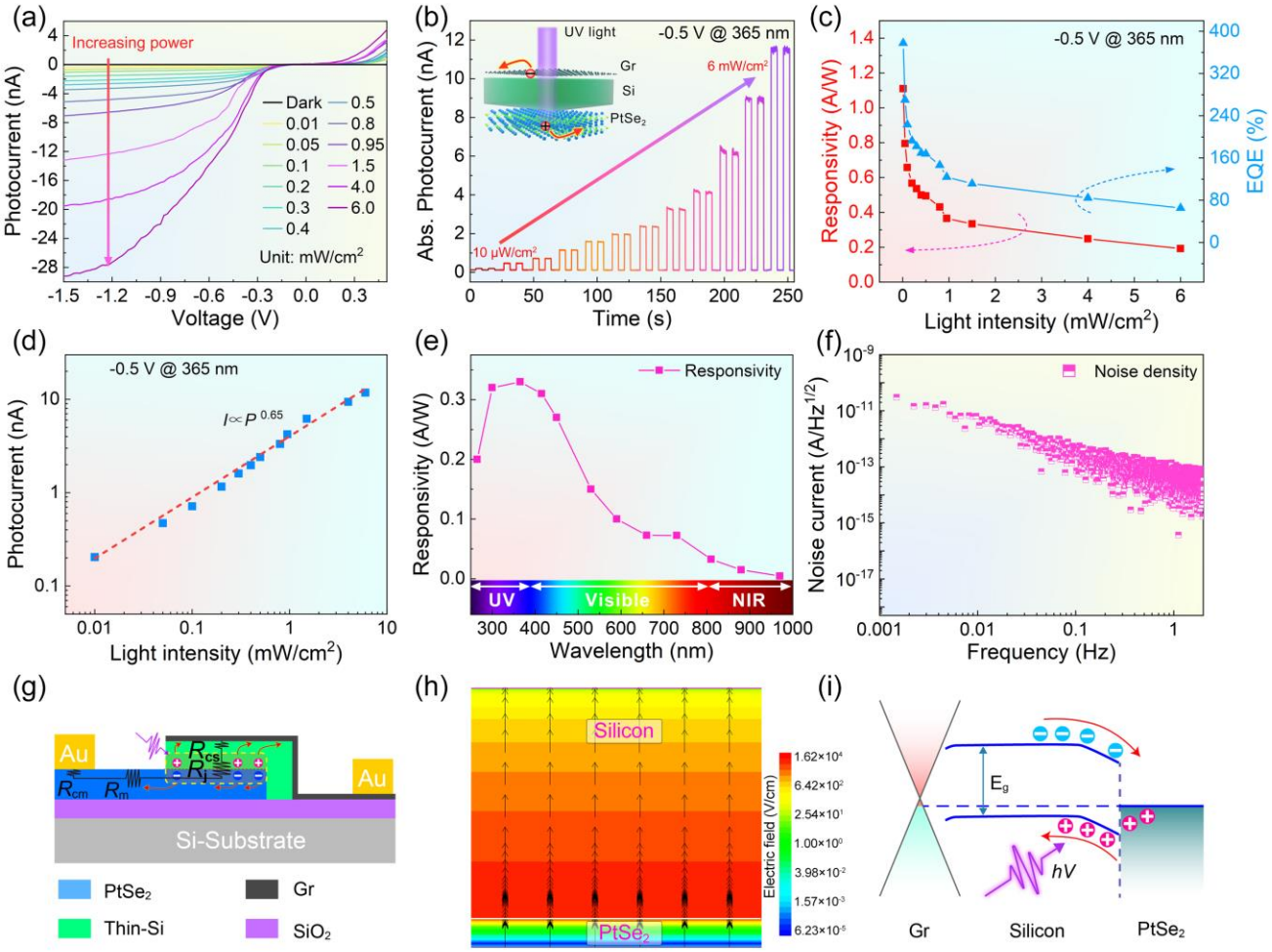

Figure 4. (a) I-V characteristics of $PtSe_2$/ultrathin-Si UVPD under 365 nm light illumination with different light intensity. (b) I-t response of the device under 365 nm illumination. The inset shows the schematic illustration of the side view of the device. (c) The light intensity dependent responsivity and EQE of the device under 365 nm illumination at -0.5 V bias. (d) Relationship between the photocurrent and the different incident light intensity. (e) The responsivity of the $PtSe_2$/ultrathin-Si UVPD under light illumination at different wavelengths from UV to NIR (1.5 mW/cm^2). (f) Measured noise current spectral density of the device as a function of frequency under -0.5 V. (g) Schematic diagram showing the simplified device model of the vertically stacked $PtSe_2$/ultrathin-Si UVPD. (h) Simulated electric

field distribution of the device. (i) Energy band diagrams of the $PtSe_2$/ultrathin-Si UVPD under light illumination.

Achieving fast response time in UV detection remains a significant challenge. Beyond the inherent physical properties of WBSs, defect-related persistent photoconductivity effects and carrier recombination cause the response speed of most UVPDs to be insufficiently fast.[45, 55] Here, the response speed of the $PtSe_2$/ultrathin-Si UVPD at various frequencies was measured using an oscilloscope and a 365 nm pulsed light signal. Figure 5a displays a schematic diagram of the I-t response test, where a function generator controls the pulse signals, and an oscilloscope is used to acquire the photoresponse signals. The photoresponse of the device under -0.5 V bias and different frequency pulse signals of 365 nm (6 mW/cm^2) is shown in Figure 5b. In general, the rise (τ_r) and decay (τ_d) times are generally defined as the periods required for the photocurrent to increase (decrease) from 10% to 90% (or decrease from 90% to 10%) of its minimum (maximum) value, respectively. Figure 5c shows the normalized photoresponse at 5 kHz, and our $PtSe_2$/ultrathin-Si UVPD achieves a fast response speed of 51.8/73.6 μs, which beats many other reported WBS UVPDs, such as PGR-GaO_x Schottky diode (0.1 ms),[55] $MoS_2/SnSe_2$ heterojunction (150/234 μs),[49] Bi_2Se_3/a-Ga_2O_3/p-Si heterojunction (342/249 ms),[59] self-powered $ZnGa_2O_4$/Si (< 40 ms),[60] MSM β-Ga_2O_3 nanobelt (0.08/0.04 s),[14] and graphene/GaN heterojunction (0.5/1.12 ms).[61] The fast response time is partly due to the superior physical properties of Si (such as dielectric constant, mobility, etc.). Moreover, the vertically stacked device structure reduce the carrier transport distance to the thickness of the ultrathin silicon (~200 nm), substantially reducing the transit time and decreasing the likelihood of recombination for photogenerated carriers.[62] Furthermore, this response speed is significantly faster than that of lateral device (Figure S6), which also demonstrates the superiority of the vertical structure. The photovoltage as a function of the pulse signal frequency is shown in Figure 5d, and the 3dB frequency is defined as the modulation frequency when the photoresponse reduces to 0.707 of its maximum value, is about 6 kHz, indicating the fast response of the device. It is worth noting that the *R* and response speed of the vertical $PtSe_2$/ultrathin-Si UVPDs not only beat those of several narrow bandgap semiconductor UVPDs, such as GaAs,[63] graphene/Si NWs,[64] MSM $MAPbBr_3$,[65] and TiO_2/Si,[66] but also exceed those of some WBS devices, including $PdSe_2$/GaN,[67] β-Ga_2O_3/GaN NWs,[51] CuZnS/Ga_2O_3,[68] etc. Despite some UVPDs exhibiting excellent R, their response speeds are

relatively slow, such as ZnS/MgZnO,[10] graphene/Al_2O_3/GaN,[69] MSM β-Ga_2O_3,[70] etc. (Figure 5e). Table S2 presents the photoresponse metrics of these devices reported in the literature and serves as a basis for performance comparison. We also investigated the stability of the$PtSe_2$/ultrathin-Si UVPD, which is well-known critical for a PD, by exposing the device to air for 4 weeks. It was observed that the device maintains high stability, with no noticeable degradation in photoresponse (Figure 5f-g). This high stability of the device is directly attributed to the excellent properties of the $PtSe_2$ nanofilm and ultrathin-Si. In addition, the top-h-BN encapsulates the device, isolating it from the air and enhancing its environmental stability.

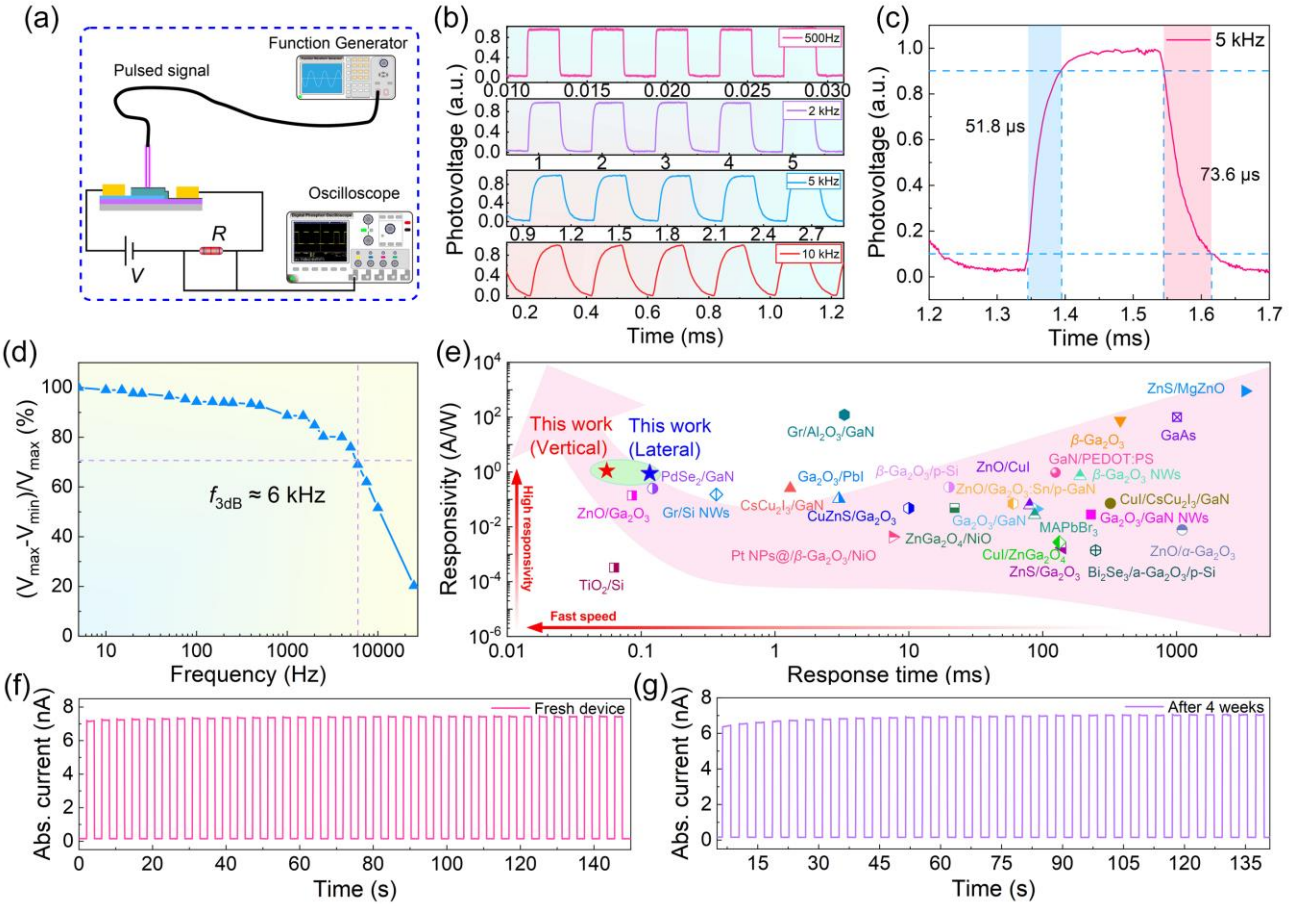

Figure 5. (a) The setup of the response speed measurement. (b) The normalized photoresponse characteristics of the device to 365 nm pulsed signals with different frequencies. (c) Response speeds under a switching frequency of 5 kHz. (d) Normalized photoresponse of the $PtSe_2$/ultrathin-Si UVPD at different pulsed light frequencies. (e) R and response time of the $PtSe_2$/ultrathin-Si UVPD compared to previously reported UVPDs. (f)-(g) Stability of the device before and after storage in air for 4 weeks.

Conclusion

In conclusion, we reported a fast UVPD based on ultrathin-Si that was obtained by wet etch exfoliated from a commercially available SOI wafer. The wafer scaled $PtSe_2$ nanofilms were selenized from the electron beam evaporated Pt film, which serves as the photogenerated electron-hole pairs fast sink. Under UV to NIR illumination, the maximum photocurrent of the device occurs in the UV region due to the large absorption of Si in this band. Theoretical simulation results suggest that ultrathin-Si is capable of completely absorbing UV light, which is attributed to the high absorption coefficient of Si in the UV range and the relatively shallow penetration depth of UV light. Moreover, the penetration depth of the incident light increases with the incident wavelength, resulting in reduced absorption by ultrathin-Si. When illuminated at 365 nm, the device demonstrates a responsivity of 1.11 A/W and fast response speed of 51.8/73.6 μs, which beats that of many WBSs-based UVPDs. This high performance is primarily attributed to the short carrier transport distance of the vertical structure and the excellent optoelectronic characteristics of Si. These results substantiate the potential application of the fast Si-based UVPD in next-generation high-speed UV optoelectronic devices.

Experimental Section

Materials Synthesis and Device Fabrication:

The preparation process for patterned $PtSe_2$ nanofilms is illustrated in Figure S2. The detailed steps for etching ultrathin-Si sheets are as follows: First, the cleaned SOI wafer was etched in a 5% HF solution for 2 h. After etching, the middle oxide layer of the SOI was removed, and the wafer was rinsed with ethanol. Next, the etched SOI was placed in a beaker filled with ethanol and subjected to ultrasonic treatment for 5 min, resulting in the formation of smaller ultrathin-Si sheets. These sheets were then dispersed onto a clean SiO_2/Si substrate and allowed to dry. Subsequently, the ultrathin-Si sheet was picked up using a PDMS transfer station. Using a 2D transfer station, The PDMS was aligned and stacked onto the patterned $PtSe_2$. Following this, graphene was transferred via mechanical exfoliation to form the top electrode. Finally, the electron beam evaporation was used to deposit a 50 nm Au film as the electrode contacts.

Materials Characterization and Device Analysis:

The surface roughness of the patterned $PtSe_2$ and thickness of the ultrathin-Si was characterized by AFM (Dimension Icon). Raman scattering spectrum was carried on laser confocal Raman

spectrometer (HORIBA) equipped with 532 nm laser. The chemical composition of $PtSe_2$ was studied by energy-dispersive X-ray spectroscopy (EDS, Oxford INCA, attached to HRTEM). The optoelectronic measurements of $PtSe_2$/ultrathin-Si UVPD were conducted using a semiconductor characterization system (2400, Keithley Co. Ltd). The different wavelengths LEDs (Thorlabs, 265, 300, 365, 415, 450, 530, 590, 660, 730, 810, 880, 970 nm) were used as light sources for the photoresponse measurements. In the test, the illumination area of the LED light source was much larger than the device area. Therefore, the effective photosensitive area used in the performance calculations was the device area. A power meter (Thorlabs GmbH., PM 100D) was used to calibrate the power intensity of incident light. The response speed of the device was evaluated by a 365 nm pulse laser diode and an oscilloscope (DPO2012B, Tektronix).

Theoretical Simulation:

The simulation of the device was accomplished using Sentaurus TCAD (Technology Computer Aided Design). SDE module was used to design the device structure. The Shockley-Read-Hall (SRH), surface recombination, and Auger recombination models were used to simulate the generation-recombination (G-R) processes of carriers transport. Ray tracing was chosen to describe the propagation of light, and the light power density of 1.5 mW cm^{-2} and irradiated perpendicular to the device surface for the simulation to match the experiments. The Si absorption simulations were conducted using COMSOL Multiphysics 5.5 via the finite-element method. A 2D simulation model was constructed with a silicon layer sandwiched between air layers (air-silicon-air), with periodic boundary conditions applied along the x direction. The structure was illuminated from the top, and the silicon thickness was varied from 250 nm to 1200 nm to analyze its impact on optical properties.

Supporting Information

Supporting Information is available from the Wiley Online Library or from the author.

Acknowledgements

This work was supported by the National Natural Science Foundation of China (62074048 and 62311530047), the Fundamental Research Funds for the Central Universities (PA2020GDKC0014,

JZ2022HGQA0185, and JZ2018HGXC0001), the Key Research and Development Plan of Anhui Province (2022f04020007), the Anhui Provincial Natural Science Foundation (2208085QF213 and 2308085MF206), the Agency for Science, Technology and Research (A*STAR) under the Career Development Fund-Seed Projects (222D800038), and the MTC Young Individual Research Grants (YIRG) (M23M7c0129).

Conflict of Interest

The authors declare no conflict of interest.

Author Contributions

J.W. conceived the research. J.W., J.Y, and B.Y. designed the experiments. J.W., Z.W., and Y.W. contributed to the device fabrication and characterizations of the materials and device. M.J. and L.L. performed the simulation. J.W., F.-X.L., and C.-Y.W. analyzed the data and wrote the manuscript. L.-B.L. and X.M. supervised the project, analyzed the results. All authors discussed the results and contributed to the preparation.

Data Availability Statement

Research data are not shared.

Keywords

Silicon-on-insulator, ultrathin-Si, UV photodetection, short channel, fast speed

References

[1] M. Razeghi, A. Rogalski, *J. Appl. Phys.* **1996**, 79, 7433.
[2] Z. Hu, Z. Li, L. Zhu, F. Liu, Y. Lv, X. Zhang, Y. Wang, *Optics letters* **2012**, 37, 3072.
[3] M. R. Hasan, T. Xie, S. C. Barron, G. Liu, N. V. Nguyen, A. Motayed, M. V. Rao, R. Debnath, *APL Mater.* **2015**, 3, 106101.
[4] D. Guo, X. Wang, H. Wang, W. Song, H. Chen, M. Qi, X. Luo, X. Luo, G. Li, G. Qin, S. Li, *ACS Photonics* **2018**, 5, 4810.
[5] Z. Li, Y. Cheng, Y. Xu, Z. Hu, W. Zhu, D. Chen, Q. Feng, H. Zhou, J. Zhang, C. Zhang, Y. Hao, *IEEE Electron Device Lett.* **2020**, 41, 1794.
[6] F. P. García de Arquer, A. Armin, P. Meredith, E. H. Sargent, *Nat. Rev. Mater.* **2017**, 2, 1.
[7] Q. Zhang, N. Li, T. Zhang, D. Dong, Y. Yang, Y. Wang, Z. Dong, J. Shen, T. Zhou, Y. Liang, W. Tang,

Z. Wu, Y. Zhang, J. Hao, *Nat. Commun.* **2023**, 14, 418.
[8] J. Q. Ng, Q. Wu, L. K. Ang, Y. S. Ang, *Appl. Phys. Lett.* **2022**, 120.
[9] H. Yu, Q. Liao, Z. Kang, Z. Wang, B. Liu, X. Zhang, J. Du, Y. Ou, M. Hong, J. Xiao, Z. Zhang, Y. Zhang, *Small* **2020**, 16, e2005520.
[10] Y. Zhu, Y. Zhang, L. Yan, D. Zhang, J. Zhou, S. Adimi, S. Ruan, *J. Alloys Compd.* **2020**, 832, 155022.
[11] Z. Xu, C. Wu, A. Li, Y. Ma, G. T. Fei, M. Wang, *IEEE Electron Device Lett.* **2018**, 39, 240.
[12] H. Zhang, F. Liang, K. Song, C. Xing, D. Wang, H. Yu, C. Huang, Y. Sun, L. Yang, X. Zhao, H. Sun, S. Long, *Appl. Phys. Lett.* **2021**, 118, 242105.
[13] Y.-C. Chen, Y.-J. Lu, C.-N. Lin, Y.-Z. Tian, C.-J. Gao, L. Dong, C.-X. Shan, *J. Mater. Chem. C* **2018**, 6, 5727.
[14] X. Zou, D. Xie, Y. Sun, C. Wang, *Nano Res.* **2022**, 16, 5548.
[15] S. Rathkanthiwar, A. Kalra, R. Muralidharan, D. N. Nath, S. Raghavan, *IEEE Trans. Electron Devices* **2020**, 67, 4281.
[16] X. Zhao, D. Jiang, M. Zhao, Y. Duan, *Adv. Opt. Mater.* **2021**, 9, 2002023.
[17] Z. Mu, Q. Zheng, R. Liu, M. W. I. Malik, D. Tang, W. Zhou, Q. Wan, *Adv. Electron. Mater.* **2019**, 5, 1800770.
[18] Z. Li, T. Yan, X. Fang, *Nat. Rev. Mater.* **2023**, 8, 587.
[19] Y. Li, J. Pan, C. Yan, J. Li, W. Xin, Y. Zhang, W. Liu, X. Liu, H. Xu, Y. Liu, *Nano Lett.* **2024**, 24, 7252.
[20] X. Chen, F. Ren, S. Gu, J. Ye, *Photonics Res.* **2019**, 7, 381.
[21] H. Dong, S. Ma, Y. Niu, Z. Yang, S. Zhang, Y. Hu, X. Hao, B. Han, G. Li, H. Dong, B. Xu, *IEEE Electron Device Lett.* **2024**, 45, 554.
[22] Z. Li, Z. Feng, Y. Xu, Q. Feng, W. Zhu, D. Chen, H. Zhou, J. Zhang, C. Zhang, Y. Hao, *IEEE Electron Device Lett.* **2021**, 42, 545.
[23] Y. Xu, X. Chen, Y. Zhang, F. Ren, S. Gu, J. Ye, *IEEE Electron Device Lett.* **2020**, DOI: 10.1109/led.2020.29988041.
[24] L. Zhang, Z. Wei, X. Wang, L. Zhang, Y. Wang, C. Xie, T. Han, F. Li, W. Luo, D. Zhao, M. Long, L. Shan, *ACS Appl. Mater. Interfaces* **2023**, 15, 14513.
[25] L.-C. Tien, Y.-C. Shih, C.-Y. Chen, Y.-T. Huang, R.-S. Chen, *J. Alloys Compd.* **2021**, 876, 160195.
[26] C. Y. Wu, M. Wang, J. Li, Y. Le, W. Fei, J. G. Hu, D. Wu, Y. X. Zhou, L. B. Luo, *Small* **2022**, 18, 2200594.
[27] Y. Zheng, X. Tang, W. Wang, L. Jin, G. Li, *Adv. Funct. Mater.* **2020**, 31, 2008307.
[28] R. Cao, Y. Zhang, H. Wang, Y. Zeng, J. Zhao, L. Zhang, J. Li, F. Meng, Z. Shi, D. Fan, Z. Guo, *Nanophotonics* **2020**, 9, 2459.
[29] J.-Y. Liu, J.-J. Wang, D.-H. Lin, J. Wang, C. Fu, F.-X. Liang, X. Li, Z.-P. Gu, D. Wu, L.-B. Luo, *ACS Appl. Mater. Interfaces* **2022**, 14, 32341.
[30] J. Miao, Z. Xu, Q. Li, A. Bowman, S. Zhang, W. Hu, Z. Zhou, C. Wang, *ACS Nano* **2017**, 11, 10472.
[31] S. Yuvaraja, V. Kumar, H. Dhasmana, A. Kumar, A. Verma, V. K. Jain, *J. Mater. Sci.-Mater. Electron.* **2019**, 30, 7618.
[32] Y. Guan, G. Cao, X. Li, *Appl. Phys. Lett.* **2021**, 118.
[33] C. Liu, J. Guo, L. Yu, J. Li, M. Zhang, H. Li, Y. Shi, D. Dai, *Light Sci. Appl.* **2021**, 10, 123.
[34] W. Bogaerts, L. Chrostowski, *Laser & Photonics Reviews* **2018**, 12.
[35] X. Ma, Q. Liu, D. Xu, Y. Zhu, S. Kim, Y. Cui, L. Zhong, M. Liu, *Nano Lett.* **2017**, 17, 6961.
[36] K. Zhang, M. Yan, H. Zhang, H. Huang, M. Arita, Z. Sun, W. Duan, Y. Wu, S. Zhou, *Phys. Rev. B*

2017, 96, 125102.
[37] Y. Lian, J. Han, M. Yang, S. Peng, C. Zhang, C. Han, X. Zhang, X. Liu, H. Zhou, Y. Wang, C. Lan, J. Gou, Y. Jiang, Y. Liao, H. Yu, J. Wang, *Adv. Funct. Mater.* **2022**, 32, 2205709.
[38] Y. Zou, Z. Zhang, J. Yan, L. Lin, G. Huang, Y. Tan, Z. You, P. Li, *Nat. Commun.* **2022**, 13, 4372.
[39] L. Wang, H. Luo, H. Zuo, J. Tao, Y. Yu, X. Yang, M. Wang, J. Hu, C. Xie, D. Wu, L. Luo, *IEEE Trans. Electron Devices* **2020**, 67, 3211.
[40] N. Tavakoli, R. Spalding, A. Lambertz, P. Koppejan, G. Gkantzounis, C. Wan, R. Röhrich, E. Kontoleta, A. F. Koenderink, R. Sapienza, M. Florescu, E. Alarcon-Llado, *ACS Photonics* **2022**, 9, 1206.
[41] T. G. Chen, P. Yu, S. W. Chen, F. Y. Chang, B. Y. Huang, Y. C. Cheng, J. C. Hsiao, C. K. Li, Y. R. Wu, *Progress in Photovoltaics: Research and Applications* **2012**, 22, 452.
[42] J. Müllerová, L. Prušáková, M. Netrvalová, V. Vavruňková, P. Šutta, *Appl. Surf. Sci.* **2010**, 256, 5667.
[43] X. He, L. Zhang, W. Hong, B. Wang, F. Sun, Z. Hong, Q. Cai, Z. Sun, W. Liu, *Adv. Opt. Mater.* **2023**, 11, 2300319.
[44] S. Yang, P. Luo, F. Wang, T. Liu, Y. Zhao, Y. Ma, H. Li, T. Zhai, *Small* **2022**, 18, e2105211.
[45] T. Hu, L. Zhao, Y. Wang, H. Lin, S. Xie, Y. Hu, C. Liu, W. Zhu, Z. Wei, J. Liu, K. Wang, *ACS Nano* **2023**, 17, 8411.
[46] F. Wang, Z. Liu, T. Zhang, M. Long, X. Wang, R. Xie, H. Ge, H. Wang, J. Hou, Y. Gu, X. Hu, Z. Song, S. Wang, Q. Dong, K. Liao, Y. Tu, T. Han, F. Li, Z. Zhang, X. Hou, S. Wang, L. Li, X. Zhang, D. Zhao, C. Shan, L. Shan, W. Hu, *Adv. Mater.* **2022**, 34, 2203283.
[47] C. Zhang, X. Yin, G. Chen, Z. Sang, Y. Yang, W. Que, *ACS Photonics* **2023**, 10, 790.
[48] C. Jia, S. Wu, J. Fan, C. Luo, M. Fan, M. Li, L. He, Y. Yang, H. Zhang, *ACS Nano* **2023**, 17, 6534.
[49] Y. Yu, T. Shen, H. Long, M. Zhong, K. Xin, Z. Zhou, X. Wang, Y. Y. Liu, H. Wakabayashi, L. Liu, J. Yang, Z. Wei, H. X. Deng, *Adv. Mater.* **2022**, 34, e2206486.
[50] A. Gundimeda, S. Krishna, N. Aggarwal, A. Sharma, N. D. Sharma, K. K. Maurya, S. Husale, G. Gupta, *Appl. Phys. Lett.* **2017**, 110, 103507.
[51] W. Ding, X. Meng, *J. Alloys Compd.* **2021**, 866, 157564.
[52] Q. Zhu, Y. Chen, X. Zhu, Y. Sun, Z. Cheng, J. Xu, M. Xu, *Sci. China-Mater.* **2023**, 66, 2777.
[53] X. Xiang, Z. Qiu, Y. Zhang, X. Chen, Z. Wu, H. Zheng, Y. Zhang, *J. Alloys Compd.* **2024**, 1002.
[54] S. Xie, A. Dey, W. Yan, Z. R. Kudrynskyi, N. Balakrishnan, O. Makarovsky, Z. D. Kovalyuk, E. G. Castanon, O. Kolosov, K. Wang, A. Patanè, *2D Mater.* **2021**, 8, 045020.
[55] X. Hou, Y. Liu, S. Bai, S. Yu, H. Huang, K. Yang, C. Li, Z. Peng, X. Zhao, X. Zhou, G. Xu, S. Long, *Adv. Mater.* **2024**, 36, 2314249.
[56] G. X. Liang, C. H. Li, J. Zhao, Y. Fu, Z. X. Yu, Z. H. Zheng, Z. H. Su, P. Fan, X. H. Zhang, J. T. Luo, L. Ding, S. Chen, *SusMat* **2023**, 3, 682.
[57] J. Renteria, R. Samnakay, S. L. Rumyantsev, C. Jiang, P. Goli, M. S. Shur, A. A. Balandin, *Appl. Phys. Lett.* **2014**, 104, 153104.
[58] Q. Dong, F. Wang, X. Hu, Y. Lu, D. Zhao, M. Zhang, T. Han, X. Hou, S. Wang, M. Long, L. Shan, *Appl. Phys. Lett.* **2022**, 120, 231103.
[59] Y. Han, S. Jiao, J. Jing, L. Chen, P. Rong, S. Ren, D. Wang, S. Gao, J. Wang, *Nano Res.* **2023**, 17, 2960.
[60] D. Han, K. Liu, X. Chen, B. Li, T. Zhai, L. Liu, D. Shen, *Appl. Phys. Lett.* **2021**, 118, 251101.
[61] X. Shen, D. Wang, J. Ning, B. Wang, H. Guo, C. Zhang, Y. Jia, J. Dong, X. Feng, X. Wang, J. Zhang,

Y. Hao, *Carbon* **2020**, 169, 92.
[62] Q. Lv, F. Yan, X. Wei, K. Wang, *Adv. Opt. Mater.* **2017**, 6, 1700490.
[63] Z.-X. Zhang, T. Haggren, J.-X. Li, J. Wang, Q.-L. Fang, H. H. Tan, L.-B. Luo, *ACS Appl. Nano Mater.* **2023**, 6, 9917.
[64] J.-J. Wang, C. Fu, H.-Y. Cheng, X.-W. Tong, Z.-X. Zhang, D. Wu, L.-M. Chen, F.-X. Liang, L.-B. Luo, *ACS Nano* **2021**, 15, 16729.
[65] M.-M. Liu, L.-L. Zhou, S.-F. Li, F.-X. Liang, Y. Xing, J.-Y. Li, C. Fu, Y.-Z. Zhao, D. Wu, L.-B. Luo, *IEEE Trans. Electron Devices* **2022**, 69, 5590.
[66] M. Kumar, J. Y. Park, H. Seo, *ACS Appl. Mater. Interfaces* **2021**, 13, 12241.
[67] D. Wu, M. Xu, L. Zeng, Z. Shi, Y. Tian, X. J. Li, C. X. Shan, J. Jie, *ACS Nano* **2022**, 16, 5545.
[68] Z. Lv, S. Yan, W. Mu, Y. Liu, Q. Xin, Y. Liu, Z. Jia, X. Tao, *Adv. Mater. Interfaces* **2022**, 10, 2202130.
[69] Q. Liu, W. Song, X. Wang, Z. Zhao, C. Zhou, K. Chen, S. Zhan, F. Gao, S. Li, *Carbon* **2023**, 201, 1061.
[70] C. Zhang, K. Liu, Q. Ai, X. Sun, X. Chen, J. Yang, Y. Zhu, Z. Cheng, B. Li, L. Liu, D. Shen, *Materials Today Physics* **2023**, 33, 101034.